Theses and Dissertations

1-1-2013

Thermal Infrared Imaging: Instrumentation and Method Development

Wayne O'Brien
University of South Carolina

Recommended Citation

Thermal Infrared Imaging: Instrumentation and Method Development

by

Wayne L. O'Brien

Bachelor of Science
Dalton State College, 2011

Submitted in Partial Fulfillment of the Requirements

For the Degree of Masters of Science in

Chemistry & Biochemistry

College of Arts and Sciences

University of South Carolina

2013

Accepted by:

Michael Myrick, Director of Thesis

John Ferry, Reader

Lacy Ford, Vice Provost and Dean of Graduate Studies

DEDICATION

This thesis is dedicated to my grandfather, William "Pete" Thompson. I grew up with memories of him but very little conversation. Later in life, I learned all about his past: being a Christian, WWII POW, a craftsman, a mechanic, a husband, a father, a friend, and a grandfather. I will always strive to follow your example in creed, integrity, wit, and compassion.

ACKNOWLEDGEMENTS

On my academic career, I have many individuals to thank. First, I am blessed to be in this position because of the Lord. I have followed Christ's example to the best of my ability and I will never cease striving to be more like Him.

My parents and sisters have been an important role of encouragement. My mother, Nancy Gent, is always there to help me through harder days while my father, Ken O'Brien, always gives me truthful advice for any situation, rather large or minute. Both parents have taught me countless factoids about life. I am very blessed to have wonderful parents. My sisters have encouraged me to push through the science, answer my weird medical questions, share common interests, and allowed for relaxing visits home. Britney Redpath, you have supported me every day and every night. Your smile and your encouraging words have kept me inspired to keep pushing to achieve something more. I am honored and blessed to call you my friend and my significant other. My friends from my hometown life: John Lobb, Michael Ferguson, Tanner Waters, and many more; thank you for support into push myself to achieve the next step in my career. My friends from graduate school: Stephanie DeJong, Shawna Tazik, Justin Copeland, David Arenivar, Audrey Duke, and more; thank you for support and enduring me over the few years we have known each other. You all have taught me too many things to list and have helped me evolve into a better person and a better scientist.

To my academic mentors; Dr. Michael Myrick, I am especially grateful for your guidance and knowledge that you have bestowed upon me. I have increased my

knowledge as both a scientist and individual. He identified the areas where I excel and where I fail; he has critique them to expect the best out of me. I will carry the he has taught me for the rest of my professional career. To Dr. Dean Turner, thank you enduring the many trips to your office, the career advice, and knowledge you gave me within the chemistry world. Your mentoring has helped me on a tremendous scale. Dr. Richard Collison, not to be confused with Dr. Collision or Santa Claus, thank you for exposing me to the world of chemistry and offering me the opportunity to be the first Bachelor of Science in chemistry from Dalton State. Thank you for the many days of sitting in your office asking you random questions concerning white phosphorous or identifying the longest carbon chain.

To my professional work mentors, Don Henson and Regina Loveless: thank you for the many years of employment, teaching the principles of operating a business, and developing my work ethic.

ABSTRACT

A recent development thermal infrared camera system was improved by designing new components to downsize physical aspect and improve the instrument's performance. A new thermal infrared light source was developed and characterized. It is designed from a custom-made Macor backpiece that holds an alumina screw. High resistance wire is coiled around the screw. The coiled wire is covered with an alumina coating. Most light sources have a spectral emissivity similar to that of a blackbody emitter. This source has a spectral irradiance profile that is not similar to a blackbody source. Thus, the lamp has an improved efficiency in the thermal infrared region.

The thermal infrared camera's microbolometer detector was calibrated for its response at specific wavelengths. An infrared camera responds with a single value that is the sum of all detectable wavelengths. This was done by developing a method to determine the spectral response from the camera a given wavelength. At 8 μm, the camera's response is an instant onset; yet at longer wavelengths, the camera's response diminishes at a slower rate.

A technique has been discovered that identifies differences on a surface using a thermal infrared camera. This technique exploits differences in polarity and heat capacity by exposing the surface to hot water vapor. We demonstrate this by showing the application of identifying blood on fabrics. Bloodstains that are diluted more than 20x are barely or not visible to the human eye. Our method uses a handheld steamer and a thermal infrared camera to observe the adsorption of water vapor. With sensitive thermal

cameras, a small increase in temperature can easily be detected: this leads to visual contrast when observing the thermographic movie. Evidence suggests that the change in temperature is due to differential adsorption of water vapor.

TABLE OF CONTENTS

LIST OF FIGURES

CHAPTER 1

INTRODUCTION

1.1 INTRODUCTION TO THERMAL INFRARED IMAGING

Instrumentation in every industry is constantly evolving to keep up with the ever changing samples and arising challenges within every respective field. Some instruments have developed over centuries and some are still in early stages of invention. The important factor when redesigning an instrument is how a new component affects the instrument's performance. The work presented here is focused on one specific purpose: to improve and enhance thermal infrared (IR) imaging of latent stains at crime scenes. This includes improvements in instrumentation, understanding one type of detector used in this process, and the early investigations of a new technique discovered that detects latent stains.

Infrared thermography is used for many applications. An infrared camera has been used a chemical vapor detector; some systems are equipped with filters fabricated to isolate specific adsorption bands (1, 2). IR thermography has been applied to medicinal applications because of its ability to detect minute temperature differences (3-5). Other applications include using IR cameras for engineering and building applications (6-8). There are two types of thermography: active and passive. Passive thermography images a surface without an external stimulus being applied to the situation (9). This technique can be used by masonry to identify hidden architecture feature. Active thermography techniques use an external stimulus, such as a light source or heating an object, which

1

induces a temperature change (9). Both of these techniques are used to gather information about objects without contaminating or manipulation.

Our research is focused using a thermal infrared camera system to identify blood and other biological stains at crime scenes. An instrument was developed, which is described by Brooke *et. al.*, that is capable of imaging blood with dilutions as low as 1:100. This work has focused on improving and calibration specific components of that instrument; specifically, a new light source is fabricated that is more efficient in the thermal infrared region and a process to calibrate a thermal infrared camera for its spectral response. And this work will include a new technique that has developed that aids in identifying latent prints on fabrics. These advances in thermal infrared imaging and method of detecting latent prints will allow future developments in thermal IR imaging.

BIBLIOGRAPHY

1. Althouse, M.L.G.; Chang, C.I. Chemical vapor detection with a multispectral thermal imager. *Optical Engineering*. **1991**, 30, 1725-1732.

2. Safitri, A.; Mannan, M.S.; Methane Gas Visualization Using Infrared Imaging System and Evaluation of Temperature Dependence of Methane Gas Emissivity. *Industrial & Engineering Chemistry Research*. **2010,** 49, 3926-3935

3. Arora, N.; Martins, D.; Ruggerio, D.; Tousimis, E.; Swistel, A.J.; Osborne, M.P.; Simmons, R.M. Effeictiveness of a noninvasive digital infrared thermal imaging system in the detection of breast cancer. *The American Journal of Surgery*. **2008**, 196, 523-526.

4. Rich, P.B.; Dulabon, G.R.; Douillet, C.D.; Listwa, T.M.; Robinson, W.P.; Zarzaur, B.L.; Pearlstein, R.; Katz, L.M. Infrared Thermography: A rapid, portable, and accurate technique to detect experimental pneumothorax. *Journal of Surgical Research*. **2004**, 120, 163-170.

5. Salaimeh, A.A.; Campion, J.J.; Gharaibeh, B.Y.; Evans, M.E.; Saito, K. Real-time quantification of Staphylococcus aureus in liquid medium using infrared thermography. *Infrared Physics & Technology*. **2012**, 55, 170-172.

6. Ummenhofer, T.; Medgenberg, J. On the use of infrared thermography for the analysis of fatigue damage processes in welded joints. *International Journal of Fatigue.* **2009**, 31, 130-137.

7. Fan, J.; Guo, X.; Wu, C. A new application of the infrared thermography for fatigue evaluation and damage assessment. *International Journal of Fatigue*. **2012,** 44**,** 1-7.

8. Madruga, F.J.; Gonzalex, D.A.; Mirapeix, J.M.; Lopez Higuera, J.M.Application of infrared thermography to the fabrication process of nuclear fuel containers. *NDT&E International*. **2005,** 38, 397-401.

9. Mercuri, F.; Zammit, U.; Orazi, N.; Paoloni, S.; Marinelli, M.; Scudieri, F. Active Thermography applied to the investigation of art and historic artefacts. *Journal of Thermal Analysis and Calorimetry*. **2011**, 104, 475-485.

10. Brooke, H.; Baranowski, M.R.; McCutcheon, J.N.; Morgan, S.L.; Myrick, M.L. Multimode Imaging in the Thermal Infrared for Chemical Contrast Enhancement. Part 1: Methodology. *Anal Chem.* **2010**, 82, 8412-8420.

11. Brooke, H.; Baranowski, M.R.; McCutcheon, J.N.; Morgan, S.L.; Myrick, M.L. Multimode Imaging in the Thermal Infrared for Chemical Contrast Enhancement. Part 2: Simulation Driven Design. *Anal. Chem.* **2010**, 82, 8421-8426.

12. Brooke, H.; Baranowski, M.R.; McCutcheon, J.N.; Morgan, S.L.; Myrick, M.L. Multimode Imaging in the Thermal Infrared for Chemical Contrast Enhancement. Part 3: Visualizing Blood on Fabrics. *Anal. Chem.* **2010**, 82, 8427-8431.

13. Brooke, H. Bridging the Modeling-Sampling Gap of Mid-Infrared Reflectance Spectroscopy of Small Particles, Films, and Fibers. Ph.D. Dissertation, University of South Carolina, Columbia, SC, 2010.

14. James D. Ingle and Stanley R. Crouch. Spectrochemical Analysis. Prentice Hall, Englewood Cliffs, 1988

CHAPTER 2

INFRARED LIGHT SOURCE

2.1 INTRODUCTION

Infrared (IR) light sources have evolved over the past two centuries since the discovery of infrared radiation in sunlight (1). The first intentionally man-made source of infrared radiation for radiant energy studies was the Leslie cube, developed in 1804 (2, 3). Macedonio Melloni used a variety of objects heated in alcohol flames as infrared sources in 1835 (4). The Bunsen burner was invented in 1855 (5) and was used by Kirchhoff as an infrared light source (6, 7), which was common until the carbon filament lamp was invented in 1880. In 1889, Knut Angstrom's measurement of the spectra of the oxides of carbon used a modified Argand oil lamp. The Welsbach gas mantle was developed in 1890 and used around the turn of the 20th century for far infrared measurements because of its good emission properties beyond 10 μm wavelength (8-10). The Nernst glower was developed for home lighting (11); it was quickly replaced for that purpose by the tungsten filament lamp, but persisted for some time as an infrared light source. This was the light source used by Coblentz in his early work on the infrared absorption spectroscopy of organic compounds (12). The most common source in use for infrared spectroscopy today is the silicon carbide Globar, which name was trademarked in 1925 and described in 1938 by Strong (13-16).

In 2010, Brooke *et al.* showed that a conventional microbolometer-based thermal camera could be used for infrared (IR) reflectance imaging (17-19). In that work, a 1000-

4

W electrically heated hotplate was used as a light source to overcome the large blackbody emission of objects at room temperature and to provide adequate signal to noise ratio (SNR) in reflectance images. For our future work, we desired a more compact and manageable long-wave infrared source that offered the potential for portable battery powered operation. Available commercial off-the-shelf units sold as infrared sources were all relatively low power devices with high temperature blackbody emission profiles. We report here the result of our effort to fabricate a lamp that would be more efficient and powerful in the 8-14 μm wavelength region.

The major IR sources designed for benchtop IR spectrometers and infrared photometers are essentially compact high temperature sources of near-blackbody radiation, which means their maximum emission spectral intensity is shifted toward the visible region, and away from the room temperature thermal region viewed by most thermal cameras. In addition, many of the commercial sources are intended for uses in collimated optical systems, so the total power of the source is not of primary importance. For such instruments, it is the emittance of the lamp, the power per unit area, which is more important. Thermal reflectance imaging as in References 17-19, on the other hand, requires a high total power in the 8-14 micrometer wavelength region, and no commercial thermal sources are optimized in this spectral region.

Infrared LEDs have also been reported that reach the mid-infrared spectral region (20-22). To date, these are not commercially available for the thermal wavelength range and are of low power compared to the commercial blackbody sources just mentioned. Many small near-blackbody IR emitters, designed for a variety of purposes, have been developed, but are also too low in power for our application or operate at too short a

5

wavelength (23-28). Still other narrow-band infrared emitters have been developed (29, 30), but none are commercial with high total power in the 8-14 μm wavelength range. And although lasers are commercially available for this spectral window, their cost per unit power compared to a heated blackbody source is quite high (31, 32), even for the common CO_2 welding laser.

The source we present below is based on an alumina machine screw that is electrically heated using nichrome wire wound about the screw threads and inserted into a parabolic reflector. The total power of the lamp exceeds 30 W with an efficiency that is nearly twice that of blackbody emitters in the thermal wavelength band. Approximately 5 of these lamps provide equivalent irradiance in the 8-14 μm band to the 1000 W hotplate source used previously.

2.2 DESCRIPTION OF IR SOURCES

The original source used in Reference 17-19 was a GE 1000 W hotplate (Model 169215) with a black coated surface rather than an exposed heating coil; it can be purchased from a number of consumer retailers. In experiments reported below, the hotplate was operated at its highest power.

The Hawkeye Technologies IR-18 (Figure 2.1A) is a silicon nitride source that encased in a 25.4-mm-diameter aluminum parabolic reflector. Silicon nitride has emission profiles that similar to that of a blackbody. The manufacturer's recommended power input setting is 18W, although we tested it up to 30 W.

6
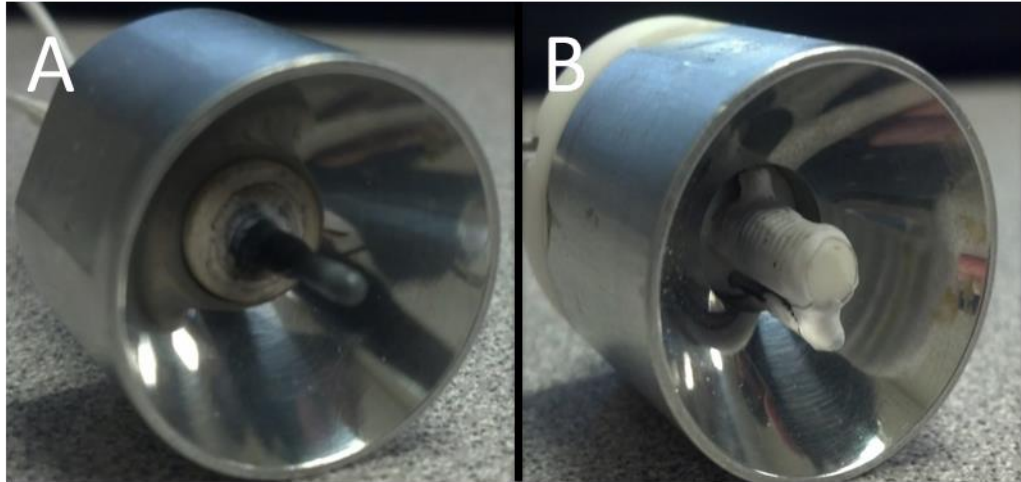
Figure 2.1 Infrared lamps evaluated in this work. (A) is the Hawkeye Technologies IR-18. (B) is the alumina lamp described in the text. A thin layer of the same alumina paste that coats the nichrome coil is used to coat the spot welds of the filament to the thicker nichrome contacts to prevent oxidation on the connection due to overheating.

The lamp that we constructed (Figure 2.1B and Figure 2.2) is based on a 25.4-mm-long #10-32 alumina screw (purchased through Amazon.com) mounted into a backplate made of the machinable ceramic Macor as a high temperature filament support. A schematic section of the lamp is shown in Figure 2.2. Two short 0.040-inch nichrome A wires run through the Macor back-piece parallel to the alumina screw to serve as electrodes. Another length of 0.010-inch nichrome A is coiled into the threads of the alumina screw to serve as a filament. Both sizes of nichrome wire were purchased from Scientific Instrument Services. The screw threads provided protection against short circuiting between loops of the filament. The ends of the coil are spot welded to the 0.040-inch nichrome electrodes. A thin layer of Ceramabond (Aremco Products, Inc), an alumina-based adhesive, is brushed over the coil and the connecting electrodes. The alumina coating is cured in an oven at 100°C. The finished filament assembly fits into a 25.4-mm-diameter parabolic reflector, MC-234 from Hawkeye Technologies, (a modified

7

version of the IR-18 mirror) and is labeled as the "alumina lamp" in Figure 2.1. Engineering drawings of the lamp are available upon request. A lamp without the alumina coating was evaluated to observe how the coating influenced the spectral irradiance.
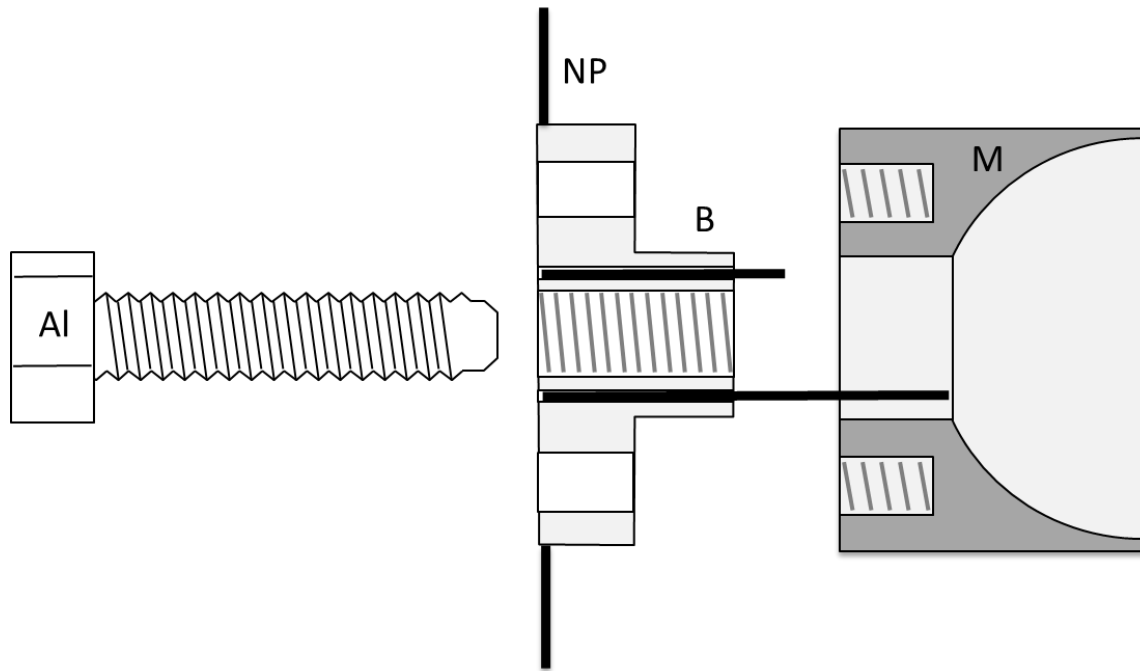
Figure 2.2. Schematic of alumina lamp. Al is an alumina screw. B is a base machined from Macor ®. NP is one of two thick nichrome posts used as contacts for the filament. M is a modifed Hawkeye Technologies 1" parabolic mirror. The posts were inserted into the Macor® base and bent into slots cut on its back, then held in place by installing the large alumina screw. The filament wire was wound around the exposed screw threads and spot welded to the nichrome posts. Alumina paste was then coated over the exposed filament and dried. The base was then inserted into the mirror and held in place with two screws. Not shown in this schematic are the filament itself, the alumina paste, and the two screws just mentioned. The components are more fully described in the text.

2.3 RADIOMETRY

The Optronics Laboratories Inc. 750-M-S system was used to determine the spectral irradiance and quantify each lamp's output. A cooled Mercury Cadmium Telluride detector (model OL 750-HSD-375) was used with a 2 second settle time and 3

8

second integration time for all measurements. The entrance and exit slits were 5 mm round apertures. A blackbody radiator (model OL 480 Variable Temperature Blackbody Calibration Standard) operating at 1200 K was used for calibration and standards in both experiments.   The software used to interface with the monochromator was OL 750 Software Applications version 1.25.

Measurements of the spectral irradiance of each lamp were made as follows. Several of the lamps tested used the same parabolic reflector mirror. For these, the center of the reflector was aligned normal to the entrance aperture of the spectrometer at a distance of 75 cm. Each lamp was evaluated at an input power of 30(±0.1) watts. The hotplate was evaluated at maximum output with the normal to the heated surface aligned opposite the normal to the spectrometer entrance slit and at a distance of 75 cm.

A performance benchmark was measured to compare the various lamps to one another. Lamps were aligned and positioned 61 cm away from a 51-mm-dia gold diffuse reflectance standard (Optronic Laboratories). The standard was observed with a thermal imaging camera (FLIR Systems, Model A315). The gold diffuse reflectance standard was observed to have a significant specular (non-diffuse) reflection that was very sensitive to alignment, so the standard was oriented to prevent the specular reflection from being inadvertently observed by the camera. Each source was modulated at 1 Hz; the small lamps were modulated with a chopper, while the hot plate was manually modulated by interposing an aluminum-foil-covered cardboard panel between the hotplate and diffuse reflector. The camera records 16-bit data at 60 frames per second through a custom LabVIEW 2012 (National Instruments, Austin TX) program; for each measurement, data was acquired for 20 seconds. The response of pixels in the image take

the form of a near-square wave as each lamp is modulated. The modulation of the signal from absorbing materials is complicated by the heating of the material caused by the lamps, which results in an increased thermal emission signal; the gold diffuse reflectance standard has very little absorption and very low emissivity and so was used to minimize heating and re-emission effects. The magnitude of modulation from a 30x25 pixel array of the standard was calculated then averaged. These values are taken as proportional to the integrated irradiance of each lamp over the thermal wavelength band observed by the camera, approximately 8-14 μm.

Since the alumina lamp was found to provide the highest overall efficiency in these tests, and also to operate at the highest power, one new lamp of this type was tested at 30 W operating input power in air for more than 1000 hours of continuous operation without failure or significant change in output.

2.4 RESULTS & DISCUSSION

A lamp used for active reflectance imaging of a large area with a thermal infrared camera needs to have significant power in the 8-14 μm wavelength range to compete with the natural thermal emission of materials at room temperature. As a comparison figure, a blackbody source at room temperature emits about 450 W/m^2, of which 170 W/m^2 is in the 8-14 μm band. Although most low-cost cameras for this wavelength region use thermal detectors whose noise is independent of signal, the reflected light intensity must still be within at least a couple of orders of magnitude of this value for acceptable reflectance imaging. Samples with low reflectance – many natural and synthetic polymer-type materials have reflectances on the order of 10% - require

10

correspondingly higher irradiance from the source to provide this level of reflected intensity.
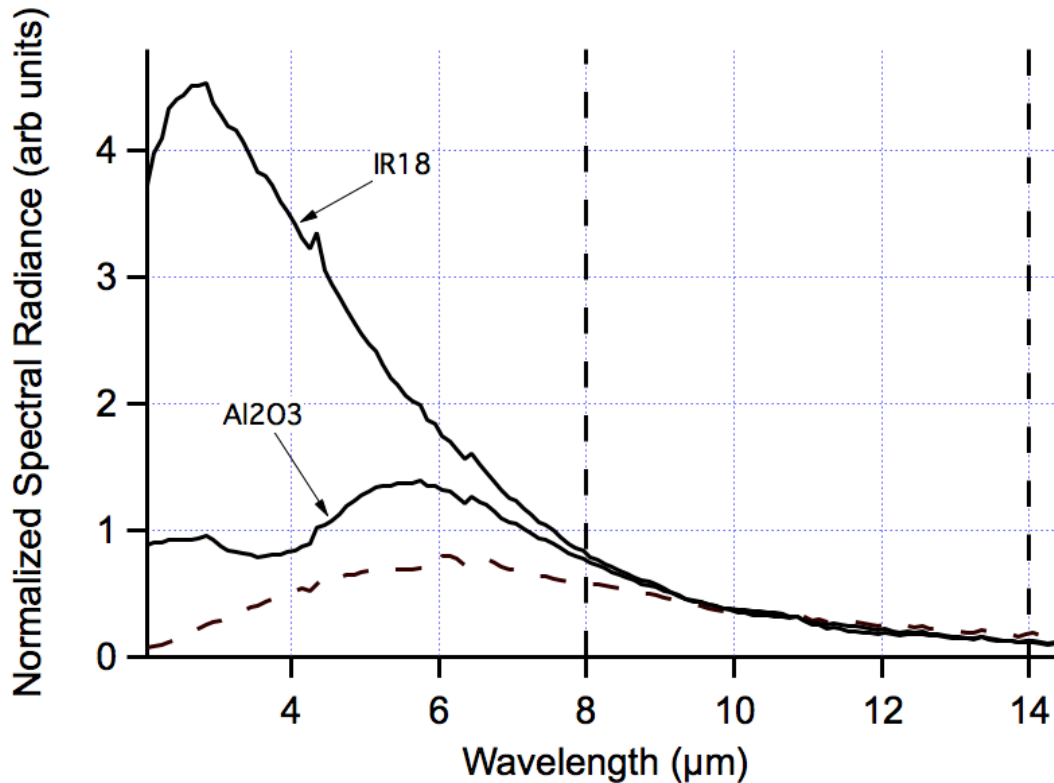
Figure 2.3 Spectral Irradiance of 3 infrared sources used in our work normalized to unit area in the 8-14 µm wavelength band viewed by a thermal camera. The dashed line is the irradiance of the hotplate infrared source. The lowest-temperature source, the hotplate, has the lowest out-of-band emission, but with low overall emission per unit area of heated surface. The higher temperature source, the commercial IR-18 lamp (top curve), has the highest out of band emission of the three tested, and fits the shape of a blackbody emission curve for 1000 K under the conditions of this test. The alumina lamp described here is also a high temperature source, but has lower out of band emission due to the low emissivity characteristic of alumina at wavelengths shorter than 5 µm.

Figure 2.3 shows the irradiance profile for each lamp located at a distance of 75 cm, with each curve having been normalized to the same area under the curve in the 8-14 µm band.

The 1000 W hotplate was operated at maximum power and was measured to have an exposed radiating surface area of 410 cm^2. The wavelength maximum for the hotplate

is near 5.9 μm and its shape is consistent with a temperature near 500 K. As the figure illustrates, an infrared source at such a low temperature has a very high relative efficiency for the 8-14 μm wavelength range, since the normalized out-of-band emission is the lowest among the lamps studied. Unfortunately, the Stefan-Boltzmann law tells us that this is achieved at the cost of having a low emittance per unit area: although 33% of its radiation lies in the 8-14 μm band, a blackbody radiator at 500 K emits only 0.35 W/cm^2 integrated over all wavelengths.   As a result, a low temperature source requires a large emitting surface area, making modulating and directing the light more difficult. Despite the high total input power of the hotplate and good distribution of the emitted radiation in the desired wavelength band, the illumination provided by the hotplate is not very intensity because it is undirected.   The source itself is very cumbersome to use even on a laboratory bench.

Most heated sources used for infrared measurements operate at significantly higher temperatures to provide higher emittance and permit the use of physically smaller sources. The IR-18 lamp has an emission profile similar to that of a blackbody at 1000 K when run under the conditions of this test.   This source is of much lower total power than the hotplate, but because it is physically small, a small parabolic reflector can be used to direct a greater portion of their emission toward the intended target. Unfortunately, most of that increased blackbody emission is outside the wavelength region observed by long-wave thermal imaging cameras: a 1000 K blackbody source emits 5.6 W/cm^2, 16X greater than a 500 K source, but with only 11% of its optical power in the 8-14 μm band.

Blackbody radiators have profiles given by Planck's radiation law. A real material has a thermal emission spectrum that also depends on its spectral emissivity,

12

which provides an opportunity to tailor the light emission characteristics of lamps. Alumina (a common form of aluminum oxide) is nominally transparent from the UV spectral window to about 5 µm wavelength. Kirchoff's radiation law reveals that materials with very low absorptivities at any given wavelength should have correspondingly low emissivities at that wavelength, and we therefore expect that a heated alumina-based lamp should have reduced optical emission at wavelengths shorter than 5 µm. This is demonstrated in Figure 2.3 for the alumina lamp. A maximum in the emission of this lamp near 5.65 µm is observed, with a secondary maximum near 2-2.5 µm. We interpret these maxima as characteristic of the heated alumina (the 5.65 µm maximum) with residual emission directly from the nichrome filament itself (the 2 µm maximum). Tests performed on an uncoated nichrome-wound-alumina lamp (not shown) showed that the alumina coating was important to establishing a good thermal contact between the filament material and the screw, without which the nichrome filament itself dominated the emission.

Electrical energy input to a lamp is dissipated by three distinct mechanisms under steady state conditions for the purposes of evaluating these two lamps. First, the lamp dissipates energy by heating the immediate surroundings via thermal conduction and convection. The lamp also dissipates energy by the emission of electromagnetic radiation, which we can conveniently divide into "in band" and "out of band" emission as our second and third mechanisms, respectively. For a blackbody radiator near 1000 K, about 63% of all radiation is at wavelengths shorter than 5 µm. Because of the steady state energy balance required between the input power and the power dissipated by the lamp, if the out-of-band optical emission of the lamp can be reduced, and if the heating of

13

the environment is not significantly increased, the same filament temperature can be reached with less electrical heating to make the lamp more electrically efficient. By this logic, the alumina lamp should be more efficient than a blackbody lamp of approximately the same temperature for our purpose.

This is demonstrated in Figure 2.4, where we report benchmark modulation values for the hotplate, IR-18 and alumina lamp. The IR-18 and alumina lamps were operated at a range of powers shown on the bottom axis of the graph. Arrows mark the rated power of the IR-18 and the power setting at which we operate the alumina lamp. The left axis shows a measure of relative power in the band seen by one particular FLIR microbolometer-based model A315 camera (every camera is expected to vary slightly because of antireflection coating variability). The hotplate benchmark value of 1.04 units of modulation per watt of power is given as a dashed line on the figure; because it is operated at 1000W, the hotplate gave a modulation average of 1040 units in the signal of the camera under the experimental condition described above for this test.
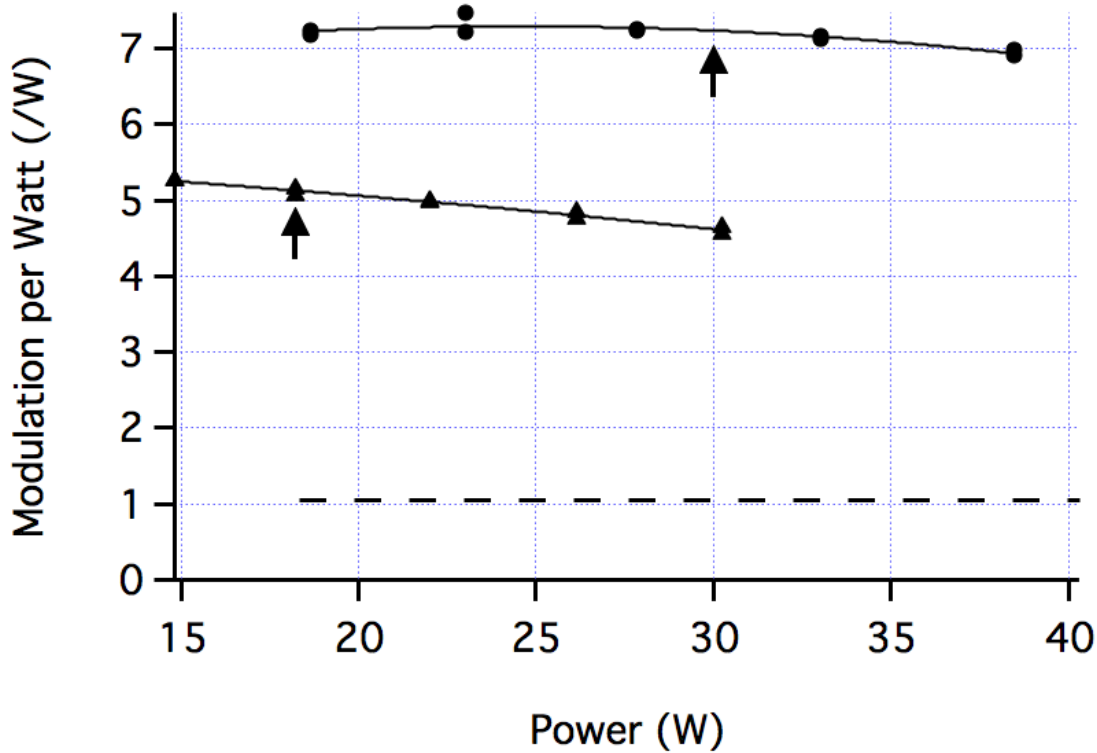
Figure 2.4 Benchmark test of the irradiance of three infrared sources as modulation in units of the 16-bit A/D signal of a FLIR Systems A315 thermal infrared camera per unit power supplied to the source. The black dashed line at the bottom shows the benchmark behavior of the hotplate used in Reference 1. The upper curve through circles is the test result for the alumina lamp described here; the middle curve through triangles is the test result for the IR-18 lamp for comparison. Arrows indicate the nominal rated power for the commercial lamp, and the 1000+ hour lifetime tested power of the homemade alumina lamp. Both of these higher temperature sources use the same parabolic reflector element while the hotplate has none, which is the main reason the hotter sources with higher out-of-band emission provide a higher modulation per watt in the 8-14 µm range than the hotplate.

The benchmark values for the IR-18 are much higher because of its parabolic mirror. At its rated power, a single IR-18 lamp produced 91.8 units of modulation. Eleven IR-18 lamps consuming 198 W would be required to provide an illumination slightly less than that of the hotplate.

The alumina lamp operating at 30 W produced 218 units of modulation. Five alumina lamps using 150 W would therefore produce a slightly greater irradiance than the 1000 W hotplate.

The results in Figures 2.3 and 2.4 appear slightly inconsistent: the power outside the 8-14 μm wavelength range appears considerably smaller for the alumina lamp than for the IR-18 in Figure 2.3, and one might expect an even higher efficiency for the alumina lamp in Figure 2.4. Results for another study (not described here) in which all the light emitted from both lamps was captured in an integrating sphere also suggests that the alumina lamp should have an output that is approximately a factor of two greater than the IR-18 in the thermal wavelength window. However, as Figure 2.1 shows, the source of the IR-18 is significantly smaller than that of the alumina lamp so that it can be more tightly collimated by the parabolic mirror. Thus, while the total output of the alumina lamp is about twice that of the IR-18 in the thermal wavelength region per unit of power supplied, the peak irradiance is only about 1.5 times greater because the irradiance is more diffuse. Still, this is an advantage in reflectance imaging because illumination by the alumina lamp is more even, with less intense hot spots, than the IR-18 provides.

2.5 CONCLUSION

We report the construction and performance of a small thermal infrared light source that takes advantage of Kirchhoff's law relating absorptivity and emissivity to increase the emission and irradiance properties of the lamp in the 8-14 μm wavelength region.

BIBLIOGRAPHY

1. Herschel, W. Experiments on the Refrangibility of the Invisible Rays of the Sun. *Royal Society of London*. **1800**, 90, 284-292.

2. Leslie, J. *An experimental Inquiry into the Nature and Propagation of Heat*; Bell and Bradfute: Edinburgh, 1804.

3. Olson, R.G. A note on Leslie's cube in the study of radiant heat. *Annals of Science*. **1969**, 25, 203-208.

4. Melloni, M. *Annal. Chim. Phys*.**1835,** 55, 337.

5. Bunsen, R.; Roscoe, H.E. Photochemische Untersuchungen. *Poggendorff's Ann. Chem. Phys*.**1957**, 100, 43-88.

6. Lockemann, G. The Centenary of the Bunsen Burner. *Journal of Chemical Education*. **1956,** 33, 20-22.

7. Kirchhoff, G.; Bunsen, R. *Poggendorff's Ann. Phys. Chem*. **1860**, 110, 161.

8. Wolfe, W.L. *Handbook of Military Infrared Technology*; Government Printing Office: Washington, DC, 1965; pp 31-56.

9. Pfund, A.H. The Electric Welsbach Lamp. *Journal of Optical Spectroscopy of America*. 1936, 26, 439-442.

10. Barnes, R.B.; Bonner, L.G.A Survey of Infra-Red Spectroscopy. *Journal of Chemical Education*. **1937,** 14, 564-571.

11. Nernst, W.; Bose, B. The theory of Auer Light. *Physics Zeits*, **1900**, 1, 289-291.

12. Coblentz, W.W. *Investigations into Infrared Spectra Part VII*. Carnegie Institution of Washington: Washington, DC, 1905.

13. Registration number 0200201 to the Wireless Resistor Company of America, now registered to Sandvik Wire and Heating Technology Corporation.

14. Strong, J Procedures in Experimental Physics (Prentice Hall Inc. New York 1938), pp 348.

15. Cann, M.W.P. Light Sources in the 0.15-20-µ Spectral Range. *Applied Optics*. **1969,** 1645-1661.

16. McCluney, R. *Introduction to Radiometry and Photometry*; Artech House: Boston, MA; 1994; pp. 79.

17. Brooke, H.; Baranowski, M.R.; McCutcheon, J.N.; Morgan, S.L.; Myrick, M.L. Multimode Imaging in the Thermal Infrared for Chemical Contrast Enhancement. Part 1: Methodology. *Anal Chem.* **2010**, 82, 8412-8420.

18. Brooke, H.; Baranowski, M.R.; McCutcheon, J.N.; Morgan, S.L.; Myrick, M.L. Multimode Imaging in the Thermal Infrared for Chemical Contrast Enhancement. Part 2: Simulation Driven Design. *Anal. Chem.* **2010**, 82, 8421-8426.

19. Brooke, H.; Baranowski, M.R.; McCutcheon, J.N.; Morgan, S.L.; Myrick, M.L. Multimode Imaging in the Thermal Infrared for Chemical Contrast Enhancement. Part 3: Visualizing Blood on Fabrics. *Anal. Chem.* **2010**, 82, 8427-8431.

20. Koerperick, E.J.; Norton, D.T.; Olesberg, J.T.; Olson, B.V.; Prineas, J.P.; Boggess. T.F. Cascaded Superlattice InAs/GaSb Light-Emitting Diodes for Operation in the Long-Wave Infrared. *IEEE Journal of Quantum Electronics*. **2011,** 47, 50-54.

21. Das, N.C. Performance Comparison of Top- and Bottom-emitting Long Wave Infrared Light Emitting Diode Devices. *Journal of Electronic Materials*. **2009,** 38, 2329-2334.

22. Das, N.C.; Bradshaw, J.; Towner, F.; Leavitt, R. Long-wave (10 µm) infrared light emitting diode device performance. *Solid-State Electronics*. **2008,** 52, 1821-1824.

23. Giraud, S.O.C.; Hasko, D.G. Mesoscale thermal infrared sources. Microelectronic Engineering. **1998,** 41-42, 579-582.

24. Bauer, D.; Heeger, M.; Gebhard, M.; Benecke, W. Design and fabrication of a thermal infrared emitter. *Sensors and Actuators A*. **1996**, 55, 57-63.

25. Laine, D.C.; Al-Jourani, M.M.; Carpenter, S.; Sedgbeer, M. Pulsed wideband IR thermal source. *IEE Proceedings-Optoelectronics*. **1997**, 144, 315-322.

26. Kwon, B.; Schulmerich, M.V.; Bhargava, R.; King, W.P. Infrared Emission from Heated Microcantilevers. *Nanoscale and Microscale Thermophysical Engineering*.

2013, 17, 141-153.

27. Yue, F.; Tomm, J.W.; Kruschke, D.; Glas, P.; Bzheumikhov, K.A.; Margushev, Z.C. PbS:Glass as broad-bandwith near-infrared light source. *Optics Express*. **2013,** 21, 2287-2295.

28. Tu, J.; Howard, D.; Collins, S.D.; Smith, R.L. Micromachined, silicon filament light source for spectrometric microsystems. *Applied Optics*. **2003,** 42, 2388-2397..

29. Inoue, T.; Asano, T.; Zoysa, M.D.; Oskooi, A.; Noda, S. Design of single-mode narrow-bandwidth thermal emitters for enhanced infrared light sources. *Applied Physics Letters*. **2013,** 30, 165-172.

30. Tsai, M.W.; Chuang, T.H.; Meng, C.Y.; Chang, Y.T.; Lee, S.C. High Performance Midinfrared narrow-band plasmonic thermal emitter. *Applied Physics Letters*. **2006,** 89, 1731161-1731163.

31. Capasso, F. High-performance midinfrared quantum cascade lasers. *Optical Engineering*. **2010,** 49, 111102-1111029.

32. Troccoli, M.; Wang, X.; Fan, J. Quantum cascade lasers: high-power emission and single-mode operation in the long-wave infrared (λ>6 μm). *Optical Engineering*. **2010,** 49, 1111061-1111069.

CHAPTER 3

THERMAL INFRARED CAMERA CALIBRATION

3.1 BACKGROUND

Whenever using an instrument to detect specific features of a measurement, the calibration and efficiency of the detector needs to be evaluated so further improvements can be implemented on the instrument. While there are many different types of detectors and different methods of calibration for each scenario, calibrating an infrared (IR) camera presents a unique challenge because IR cameras uses a focal plane array of individual detectors. Each detector, or pixel, outputs a single number that is summation of total signal: the signal is a description of all detectable wavelengths. Today, IR cameras are manufactured in large quantities and used in commercial, military, medical, and research environments (1-8).

Methods have been reported to calibrate infrared cameras for their temperature response since an IR camera's primary function is to identify temperature differences (9, 10). Calibration for a spectral response has been accomplished in a few scientific scenarios. A spectrally calibrated infrared camera was set on the side of a rocket to monitor the temperature of debris (11). The details of the method they used to determine a spectral response of the camera were not fully explained. Other methods have been used to spectrally calibrate the camera but would not be ideal for our situation because lack of detail in the spectral response curve or the method requires unavailable equipment

(12, 13). However, these techniques do offer suggestions and valuable information about IR camera systems.

Since the IR camera (FLIR A315) used in the instrument that is being developed in our laboratory did not include a spectral response calibration profile, the camera's spectral response was investigated and reported with the procedure listed below. The camera's stated wavelength response range is 7.5 to 13 μm. With this technique, the determined spectral response curve shows the camera begins to respond at 8 μm, and the response peaks at 9.6 μm; at longer wavelengths, the response decays at a relatively constant rate. This information will allow future development of a filter system that will aid in identifying latent stains: this will not be discussed here.

3.2 EXPERIMENTAL

The FLIR A315 thermal infrared camera was spectrally calibrated; it uses a 320x240 uncooled microbolometer focal plane array (14). It has a Germanium lens with an anti-reflective coating, which allows more light to be transmitted due. A Ge lens would reflect more light because of its large refractive index (RI); since the anti-reflective coating has an RI between air and germanium, this allows less light to be reflected at each interface than an air/germanium interface. The camera was operated using in-house software written in LabVIEW 2012 (National Instruments, Austin TX). In order to have the largest number of pixels illuminated by the infrared light, the camera's zoom was set to the minimum value. The temperature sensitivity range was set to -20 to +120 °C.

Chopper

IR Camera | Collimating Optics | Monochromator | IR Glower
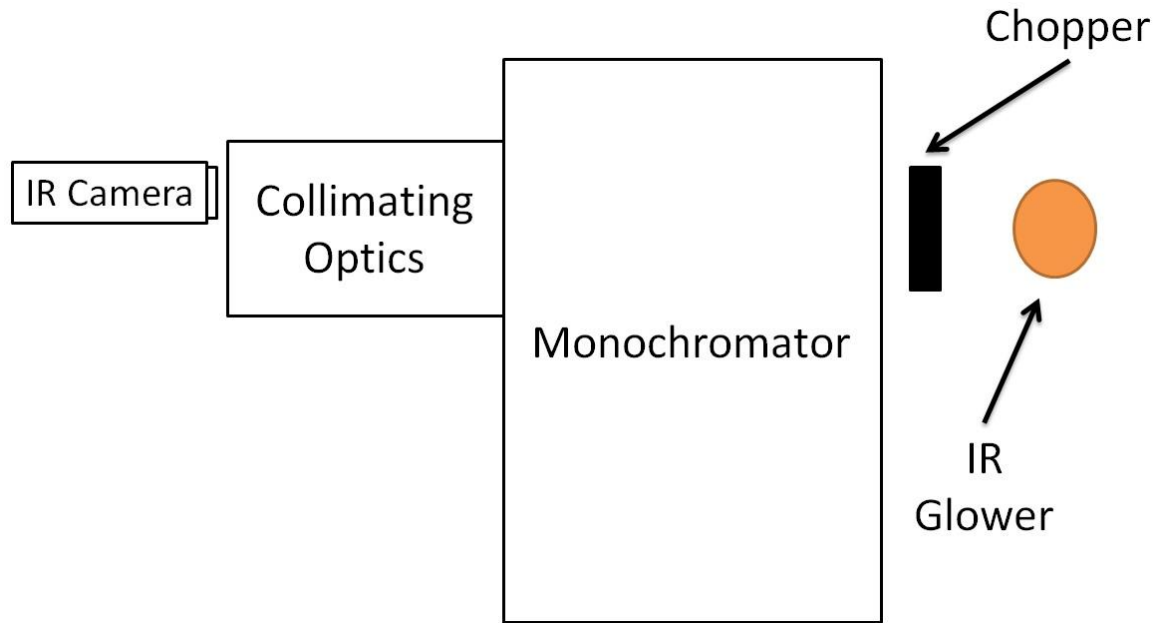
Figure 3.1 The IR camera is placed at the exit of the collimating optics. The collimating optics were not used with the standard detector. The IR glower remained in the same position during the measurement of the standard detector, but the chopper was removed.

To isolate specific wavelengths of light, a monochromator (MC), Optronic Laboratories Inc. 750-M-S, was used; 5 mm circular entrance and exit apertures were used. The LG 100-75 and LG 225-40 (both from Optronic Laboratories, Inc.) gratings were used within the MC. The IR/Visible Dual Light source attachment (Optronic Laboratories Inc., Model: 740-20D/IR) was used as the light source; the IR Glower was operated at 48 W. The standard detector used was a pyroelectric detector (Optronic Laboratories Inc., Model: OL 750-HSD-380). Collimating optics (Optronic Laboratories Inc., Model 750-10C) were used while the camera was being used as a detector. A chopper, which operates at 1 Hz and was made in-house for this experiment, was placed between the light source and the MC's entrance; the chopper was controlled by the LabVIEW program that was used to interface with the IR camera. Figure 3.1 shows the experimental setup when the camera's response was being recorded. The alternating

current (AC) was calculated at each wavelength using a separate LabVIEW program; AC image processing was explained and applied by Brook *et. al.* (15-17). The AC image was calculated to remove the background from the images. Once the AC images were calculated, they were processed using a custom Matlab that established the response number of the camera.

To measure the response of the camera from the AC images, two 70x80 pixel areas of the image were designated as the background, and an 85x80 pixel region was used as the signal area. The average pixel value was calculated for each region; the average of two background areas was subtracted from the average pixel value of the signal area. AC images were calculated from 7000 nm to 18000 nm with measurements every 100 nm. Figure 3.2 displays an image when the camera is not detecting radiation and an AC image when radiation is detected.

Once the signal was calculated a specific wavelength, the signal were ratioed to the response curve of the pyroelectric detector; this process compensated difference intensities of the light source at different wavelengths.
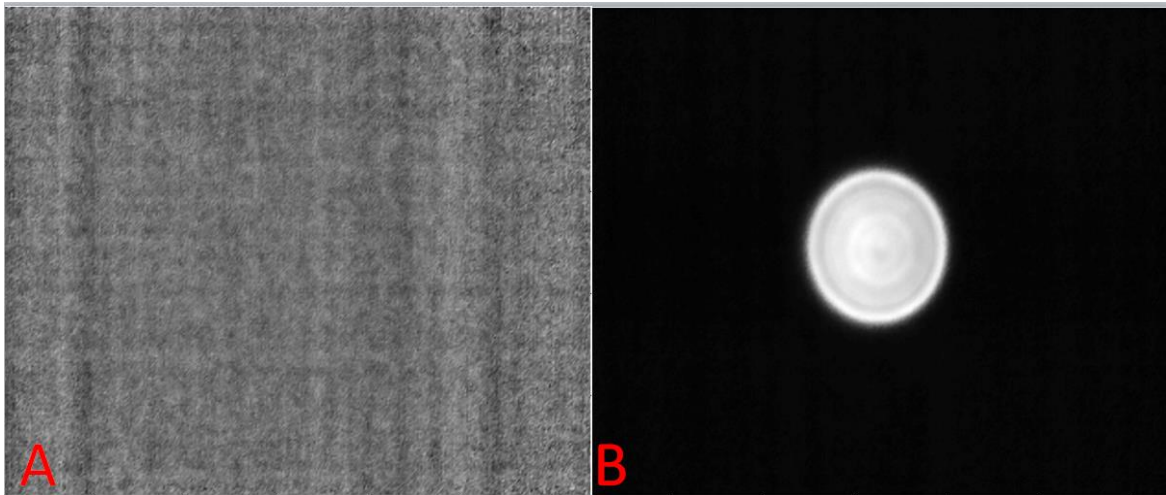
Figure 3.2 Image A is the AC image at 7600 nm; Image B is the AC image 9500 nm. In image A, there is no response observed by the camera while image B shows a high

response to the different wavelength of light. Image B shows a high response to the radiation at that wavelength: so high that the background is blacked out.

3.3 RESULTS & DISCUSSION

Figure 3.3 is the response curve for the IR camera. The camera did not observe any radiation below 7.7 µm; this is different than rated by the manufacturer. The peak sensitivity of the camera is at 9.6 µm. The IR camera begins to respond beyond 7.8 µm. The response trickles to 50% at 13.6 µm, which is the cutoff wavelength listed by the manufacture in reference 14.

The two gratings used had an overlapping region from 13.0 µm to 14.5 µm. Within this region, the two gratings had a similar trend in response but the values for the LG 100-75 (used for the wavelength region 7.0 to 14.5 µm) were at a slightly lower value. To compensate for the difference in value, the ratio of LG 225-40 (used for wavelengths beyond 13.0 µm) response to the LG 100-75 was calculated for wavelengths between 13.0 and 14.5. The correction factor was applied to all response values for the LG 225-40 grating.
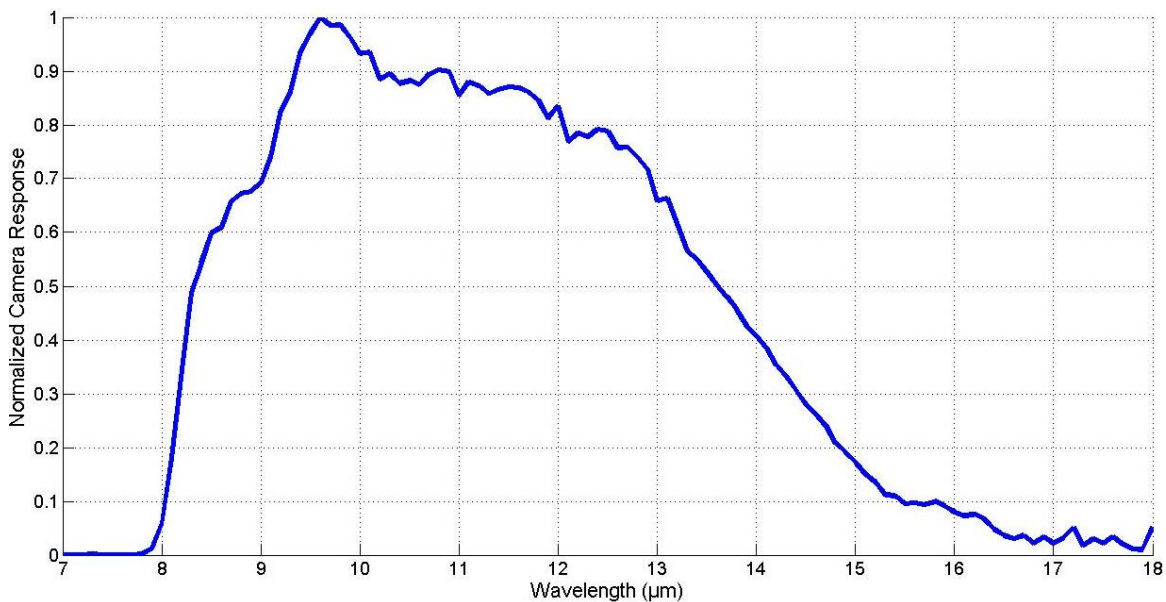
Figure 3.3 This is the response, or sensitivity, curve for the FLIR A315. From 7.0 to 14.0 μm, the LG 100-75 was used; beyond 14.0 μm, the LG-225-40 was used. This changing point was set by the MC's software and the manufacturer. The final response values were ratio to the maximum value so that the wavelength with the highest response would be equal to 1.

3.4 CONCLUSION

The response curve was calculated with the following procedure. This response range was different than the stated response range because wavelengths below 8 μm do not generate a response. This method could be adapted to be used with other cameras to determine the differences in spectral sensitivity.

BIBLIOGRAPHY

1. Rogalski, A. History of infrared detectors. *Opto-Electronics Review*. **2012**, 20(3), 279-308.

2. Kateb, B.; Yamamoto, V.; Yu, C; Grundfest, W.; Gruen, J.P. Infrared Thermal Imaging: a review of the literature and case report. *NeuroImage*. **2009**, 47, T154-T162.

3. Bagavathiappan, S.; Lahiri, B.B.; Saravanan, T.; Philip, J.; Jayakumar, T. Infrared Thermography for condition monitoring – A review. *Infrared Physics & Technology*. **2013**, 60, 35-55.

4. Verhoeven, G. Imaging the invisible using modified digital cameras for straightforward and low-cost archaeological near-infrared photography. *Journal of Archaeological Science*. **2008**, 35, 3087-3100.

5. Peng, D.; Jones, R. Lock-in thermographic inspection of squats on rail steel head. *Infrared Physics & Technology*. **2013**, 57, 89-95.

6. Lahiri, B.B.; Bagavathiappan, S.; Jayakumar, T.; Philip, J. Medical Applications of infrared thermography: A review. *Infrared Physics & Technology*. **2013**, 55,

221-235.

7. Deans, J.; Gerhard, J.; Carter, L.J. Analysis of a thermal imaging method for landmine detection, using infrared heating of the sand surface. *Infrared Physics & Technology*. **2006**, 48, 202-216.

8. Safitri, A.; Mannan, M.S. Methane Gas visualization Using Infrared Imaging System and Evaluation of Temperature Dependence of Methane Gas Emissivity. *Industrial & Engineering Chemistry Research*. **2010**, 49(8), 3926-3935.

9. Horny, N. FPA camera standardization. *Infrared Physics & Technology*. **2003**, 44, 109-119.

10. Bower, S.M.; Kou, J.; Saylor, J.R. A method for the temperature calibration of an infrared camera using water as a radiative source. *Review of Scientific Instruments*. **2009**, 80(9), 1-7.

11. Gauthier Jr., L.R.; Howser, L.M.; Prendergast, D.T.; Mattix, M.P. Radiometric dynamic scene processing for uncooled IRFPAs. In *SPIE Proceedings 1996*, Proceedings of the Infrared Imaging Systems: Design, Analysis, Modeling, and Testing XVII, Orlando, FL, April 17, 2006.

12. Mermelstein, M.D.; Snail, K.A.; Priest, R.G. Spectral and radiometric calibration of midwave and longwave infrared cameras. *Optical Engineering*. **2000**, 39, 347-352.

13. Rice, J.P.; Lykke, K.R.; Yoon, H.W. A method for testing the spectral responsivity of infrared cameras using tunable lasers. Proc. SPIE 5076, Infrared Imaging Systems: Design, Analysis, Modeling, and Testing XIV, 112 (August 25, 2003); doi:10.1117/12.487113.

14. FLIR A315 / A615 Thermal Camera Technical Specifications – FLIR. http://www.flir.com/cs/emea/en/view/?id=41955 (accessed June 27, 2013).

15. Brooke, H.; Baranowski, M.R.; McCutcheon, J.N.; Morgan, S.L.; Myrick, M.L. Multimode Imaging in the Thermal Infrared for Chemical Contrast Enhancement. Part 1: Methodology. *Anal Chem.* **2010**, 82, 8412-8420.

16. Brooke, H.; Baranowski, M.R.; McCutcheon, J.N.; Morgan, S.L.; Myrick, M.L. Multimode Imaging in the Thermal Infrared for Chemical Contrast Enhancement.

Part 2: Simulation Driven Design. *Anal. Chem.* **2010**, 82, 8421-8426.

17. Brooke, H.; Baranowski, M.R.; McCutcheon, J.N.; Morgan, S.L.; Myrick, M.L. Multimode Imaging in the Thermal Infrared for Chemical Contrast Enhancement. Part 3: Visualizing Blood on Fabrics. *Anal. Chem.* **2010**, 82, 8427-8431.

27

CHAPTER 4

LATENT HEAT THERMOGRAPHY

4.1 INTRODUCTION

Our laboratory has made advances in alternative imaging methods using an infrared camera to identify blood on fabrics (1-3). In the process, it was noticed that fabrics experienced variation in their masses because of humidity changes in the surrounding environment; this has been observed in other laboratories (4, 5).

An abundance of research has been done in different areas which encompass one or more elements of our experimental technique that we discuss. Many different techniques have been publish to study moisture content in a broad range of fabrics; these studies focus on analyzing how moisture content contributes to comfort level, water mechanics within fibers, and manufacturer properties (6-11). It has also been reported that the heat of adsorption of water is higher than expected when water is adsorbed to a sulfonic or an amino group (12). Vainer used a short wave IR camera (3-5 μm wavelength region) to identify what he described as "thermal fire": this was the process of dipping a strip of fabric into room temperature water (16-18 °C) and the wicking action caused temperature rise higher than expected (13). Most notably, he reported flannel and poplin cotton experiencing an 8°C temperature rise. In another experiment, he showed that water vapor yielded a thermal response by placing a piece of fabric above a dish filled with room temperature water. Loskyll used a shortwave infrared camera to monitor the temperature of different catalysis as they are exposed to different gases over

28

time (14). The difference in temperatures is attributed to the heat of adsorption and the heat of reaction.

With these concepts, we carried out our experiment by exposing bloodstained fabrics to steam. The results were quite unexpected because this provided a contrasting technique. We have explored this technique by applying algorithms to aid in identifying regions of interests; however, calculating the range of each pixel in time offers spatial information and provides an image that allows for areas of interest to be identified. In this chapter, example results for two fabrics with bloodstains are shown: an acrylic fabric and a polyester fabric.

4.2 EXPERIMENTAL

A Rowenta Portable Handheld Garment Steamer was used for all the experiments. It has an 800W heater to generate steam. Deionized water and NMR grade deuterium oxide (Cambridge Isotope Laboratories, Inc.) were used as sources for steam. The steamer converts water to steam at a rate of 0.16 mL of per second; this was determined experimentally by measuring the amount of water used over a period of constant operation. It is important to note that the steam is not at a high temperature to harm the sample: the author of the paper has exposed their hand to the steam only inches from the exit port without harm. To monitor the sample, the FLIR A315 Thermal Infrared camera was used. The camera records 16-bit data at 60 frames per second. The camera uses an uncooled microbolometer detector that is sensitive to the 8-14 µm wavelength region. In-house software, which was developed using LabVIEW© (National Instruments, Austin TX), was used to control the camera and record data. All measurements were done in a laboratory environment (room temperature and between 20%-40% humidity).

29

Two fabric samples were prepared using rat blood from the University Of South Carolina School Of Medicine's Animal Research Facility. The first sample is a triple dyed acrylic fabric that has 5 different dilutions of rat blood on the sample: 'I' represents neat blood, 'X' represents 10x dilute blood, 'V' represents 25X dilute blood, 'L' represents 50x dilute blood, and the 'C' represents 100x dilute blood. This sample fabric was prepared 3 years for previous experiments. The other sample is a polyester fabric with a pattern pressed onto the fabric; the fabric had two stains deposited on the surface. This type of polyester felt silky to the touch; it was not the fuzzy type of polyester material. A researcher wore a disposable nitrile glove and dipped their hand in diluted rat blood then placed their hand on the fabric. The left handprint represents blood of 100x dilute and the right represents 1000x dilute blood. At the time of steaming, the polyester's bloodstains were 4 months old. After the blood dried, the hand prints are not visible to the human eye. Both of these fabrics are show in Figure 4.1.

A fabric sample is positioned vertically; it supported by a steel backdrop. The infrared camera is 30-inches away from the surface. The handheld steamer, which never enters the camera's field of view, steams from 8-inches away from above the surface. A wave-like motion is used to apply steam.

Figure 4.1 Image A shows the acrylic fabric with a 12-inch ruler. One can observe the 'I', the 'X', and the 'V', but the other two bloodstains are not visible. Image B show the polyester fabric with the sewn-in skull prints. The bloodstains are not visible even with close examination. The skull pattern is the type that is iron onto the fabric during production.

4.3 RESULTS & DISCUSSION

Blood is composed of two primary categories: 55% plasma and 45% cellular components (15). The plasma is 90% water, which contains an assortment of dissolved salts. The remaining portion of plasma is composed of plasma proteins and substances that are transported in blood, such as nutrients and hormones. The cellular component is primarily erythrocytes, or more commonly known as red blood cells. Erythrocytes are primarily composed of hemoglobin, an iron containing protein that transports oxygen. Rat blood is used in these experiments; the solids content of rat blood has been reported to be roughly 20% by weight (16). There are a few main heating processes that can happen when steam is exposed to fabric. An enthalpy of water adsorption can be observed; these values have been studied in specific situations and differ in magnitude between types of proteins (17). The bloodstains change the number of adsorption sites and could have a more negative adsorption enthalpy than the fabric background; these

www.manaraa.com

two factors are exploited when steam is applied. The fabric's temperature will be increased by the hot vapor being exposed to the surface.

Figure 4.2 is nine images that depict the process of exposing the fabric to hot water vapor. Deuterated water was used in this experiment. Frame 1 and 300 shows a traditional passive thermographic image. The bloodstains that are visible with the human eye are observed in these images. The vapor exposure begins a few of frames before frame 600. The bottom portion of the 'X' stain has a higher intensity than the surrounding areas when the steam comes into contact with fabric's surface. This is not showing that the technique is sensitive to only blood; rather, it is sensitive to identifying differences in hydrophobic properties on the surface. In an experiment not shown, vacuum grease was applied to the same type of acrylic fabric. When exposed to the steam, the greased area did not show a response and stayed at a lower temperature than surrounding areas. In frame 900, the entire viewing region has been exposed to some amount of steam (not evenly distributed), and the latent stains are visible. There are other noticeable attributes about frame 900: drips of blood in random places (these were accidently dripped during the original staining), the 'V' stain has wicked out into the fabric area, and 'L' stain is visible in the images even though the surrounding area is dark even though it was not the focus during the experiment. Between frame 1200 and 1500, the steaming process ceases. In the 'X', the 'V', and the 'C', the inner part of the letters cools faster than outer edges that is observed in frame 1800, 2100, and 2400. In frame 2400, the ability to specifically identify areas that have latent stains is difficult because of the cooling processes. The difference in signal between the areas because smaller as the

surface re-equilibrates to its original condition. The magnitude of temperature increases is around 12-16 °C above room temperature.
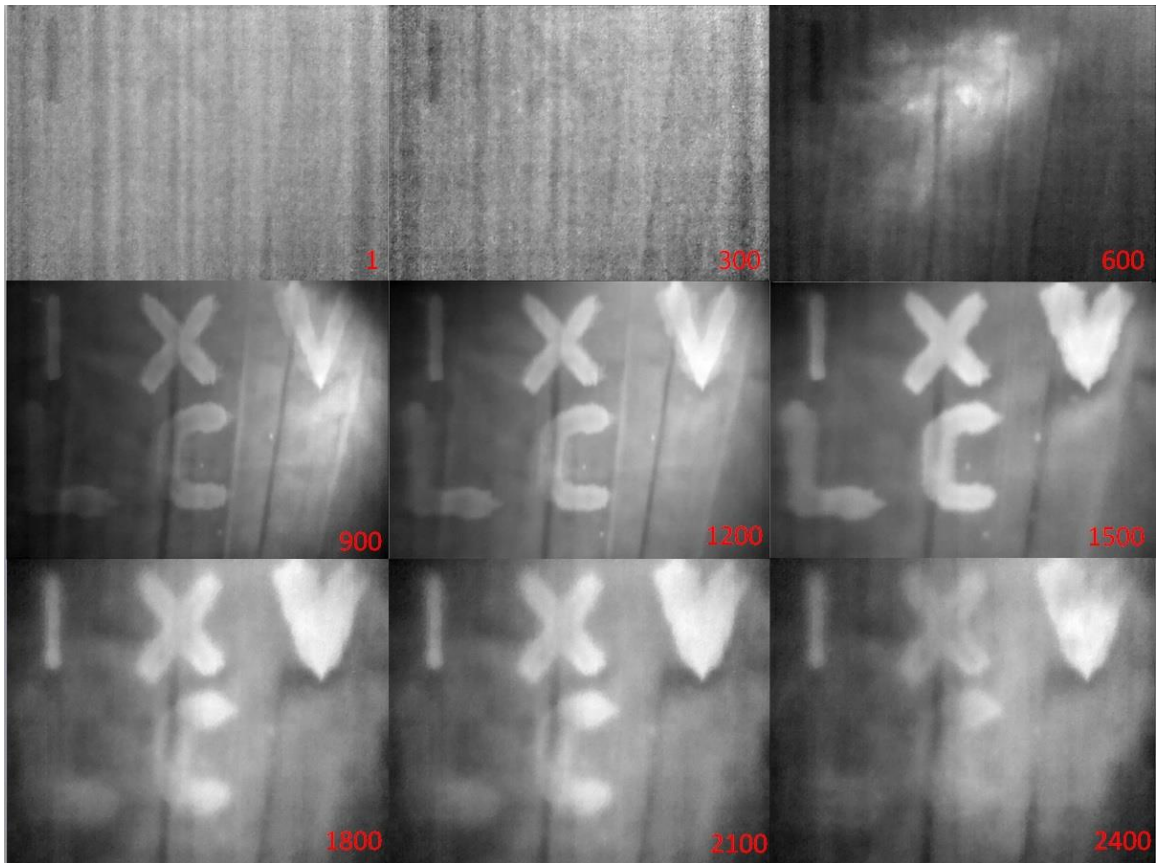
Figure 4.2 The 9 images are thermographic images taken from the FLIR A315. The red number corresponds to the frame number. The vertical lines that are observed in frame 900 and beyond are creases in the fabric. About 30 seconds after frame 2400, the fabric returns to its original condition.

Figure 4.3 shows pixel data from a small area on the fabric. Three pixels were selected: a pixel from the bottom-right portion of the 'X', a pixel between the bottom right of the 'X' and the top right of the 'C', and a pixel from the top right portion of the 'C'. These pixels were chosen because of their close proximity to each other. Even though there is a factor of 10 between the two dilutions of blood, the difference in signal is not significant. The bloodstained areas remain at a higher temperature while the neat fabric area cooling down. This can be observed in the later frames.
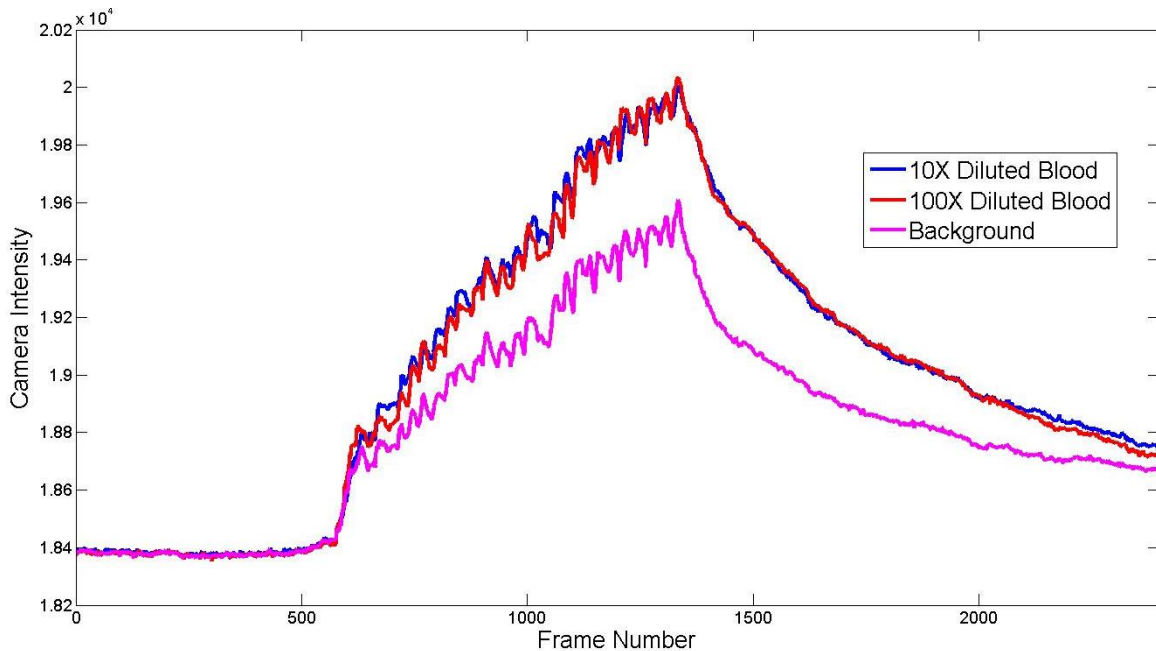
Figure 4.3 Pixel data from steaming the acrylic fabric. The pink line, listed as the background, represents the neat acrylic fabric. The red and blue lines represent the 'C' and the 'X', respectively. Notice how the fabric experiences the same oscillation as the bloodstains yet the magnitude is difference. It also appears that the bloodstained areas have a higher slope than the fabric.

The polyester fabric yielded different observations than the acrylic fabric. Figure 4.4 shows six images from the steaming process. Deionized water was used in this experiment. Frame 1 shows the typical thermographic image before steaming. Since the fabric's surface is at the same temperature, the IR camera does not show the skull print on the fabric. There are a number of creases are noticeable in the fabric; particularly, there is a horizontal crease across the upper portion of the fabric that is noticeable in frame 200. The steamer is expelling hot water vapor directly above the fabric at roughly 8-inches away. An outline of a palm is discernible; however, the large horizontal crease is blocking a large portion of the steam from the bottom portion of the fabric in that frame. Between frame 200 and 400, which is about 3 seconds in time, two hand prints are easily presented by the steaming method. The 1000x diluted handprint (which is on the right

34

side of the image) is fully visible. The 100x dilute handprint, which is not completely shown in the camera's field of view, is also visible: only the hand index finger and the thumb are visible in the IR images. In frame 600, the hand prints are not visible because the response of the fabric is similar to the response of the bloodstained areas. Steam is still being exposed to the sample until frame 630. In frame 800, portions of the bloodstained area show a cooler signal but only above the crease that was previously mentioned. The other areas exhibit a cooler signal in later frames. This is the opposite than the acrylic fabric: the bloodstains retained a higher temperature than the rest of the fabric, which is observed in 'V' stain. There are areas of exception, such as the inner portion of the 'X'. With the polyester fabric, the bloodstains cool faster than areas without blood on the surface. Figure 4.5 shows pixel data from the fabric.
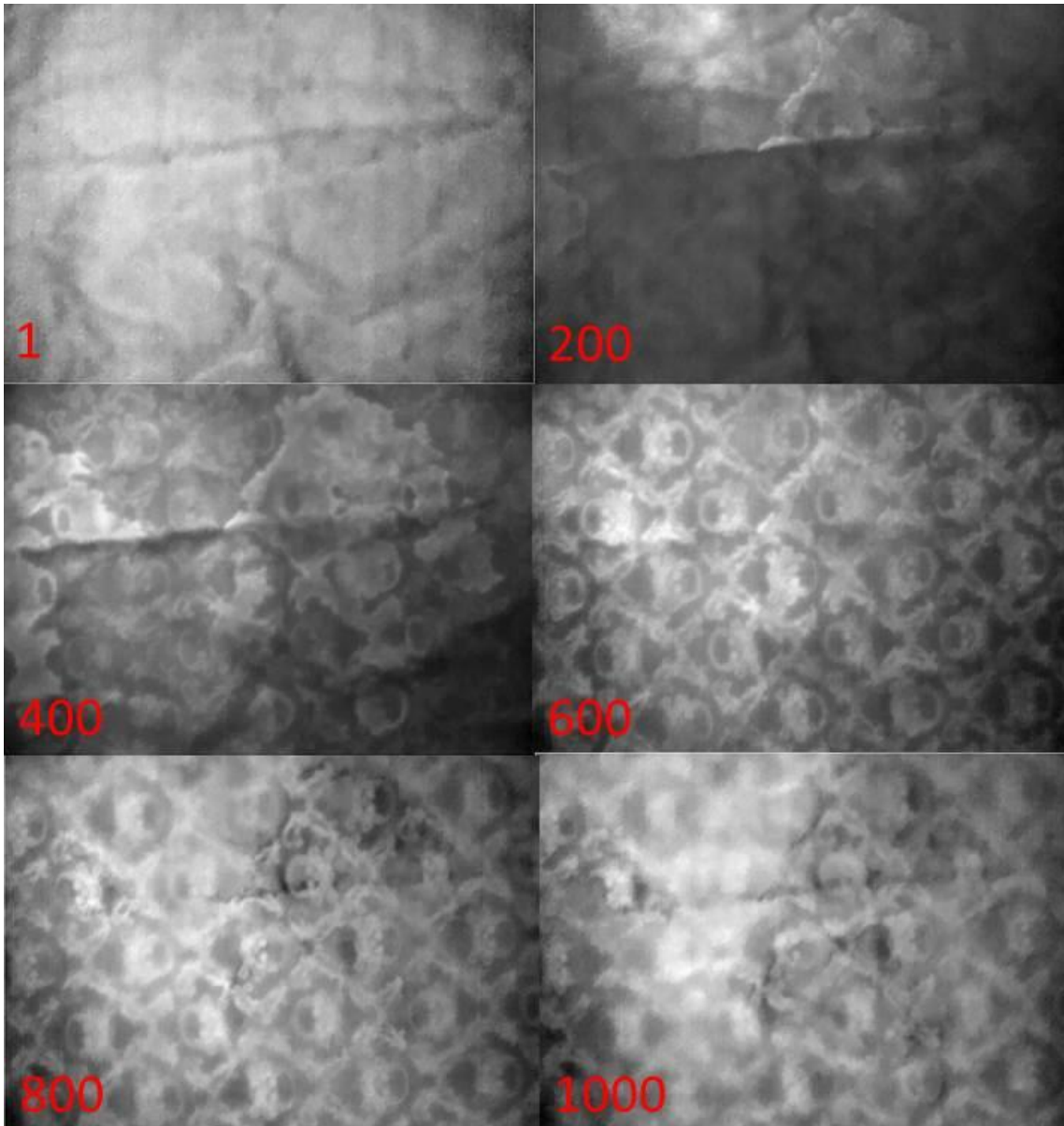
Figure 4.4 These are six images from the thermographic recording of the steaming the polyester fabric. The red numbers present the frame number. Frame 1 shows the passive thermographic image.
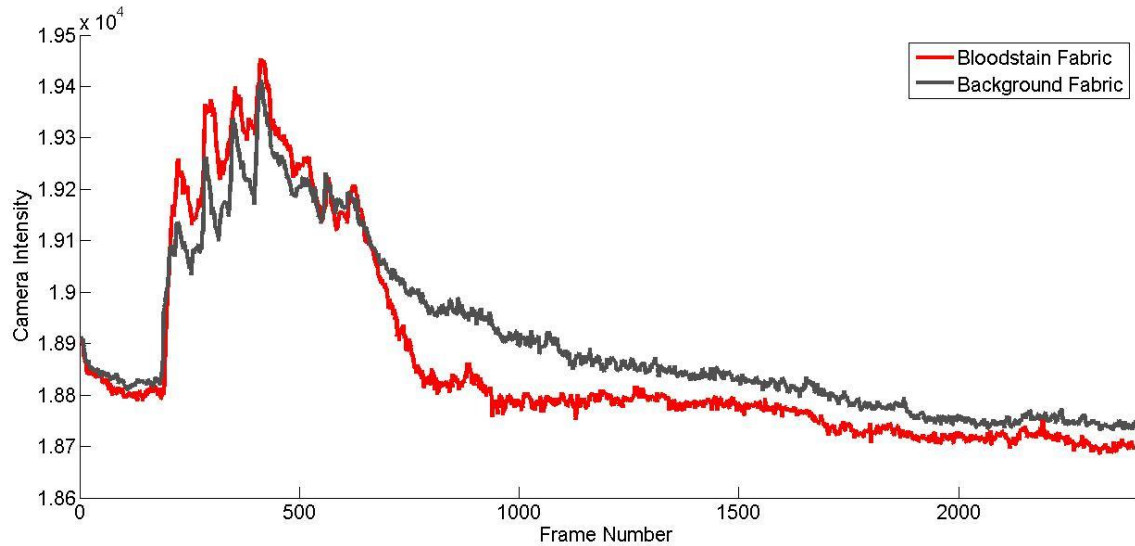
Figure 4.5 Pixel data from neat and bloodstained polyester fabric areas. These pixels were separated spatially by 1 cm. The bloodstained area shows a higher response to the steam initially, but the difference in response between the neat and bloodstained areas becomes less over time. At the end of the process, the bloodstained fabric cools to a lower temperature faster than neat the neat area as observed in Figure 4.4. This would lead to the following hypothesis: there is a small difference in the enthalpy of adsorption between blood proteins on polyester fabrics and neat polyester fabric, the blood on the surface of the fabric does not sign.

One of the main challenges with this technique is identifying a processing method that identifies areas of interest for further investigation. Most researchers do not have to time to sift through multiple thermographic movies trying to observe minor details. There have been multiple attempts at applying different data processing techniques to aid in identifying these areas of interests in the thermographic movies. Derivative processing (first and second derivatives by spatial and time domain), background subtraction, Savitzky Golay smoothing, image convolution using different kernels, and others techniques have been attempted. The problem that arises is that each measurement and sample is different from the previous. Applying a technique in a specific sample allows the experimenter to identify the specific areas of interests: the same data processing technique applied to a different sample does not identify areas of interests.

www.manaraa.com

The method, so far, that yields the best results for the majority of the steaming experiments is calculating the range of each pixel in time. This simple statistic allows for visualization of intensity differences across the entire image while spatial information is also displayed. This method was applied to the acrylic fabric and polyester fabric samples. The results of calculating the range can be seen in Figure 4.6.
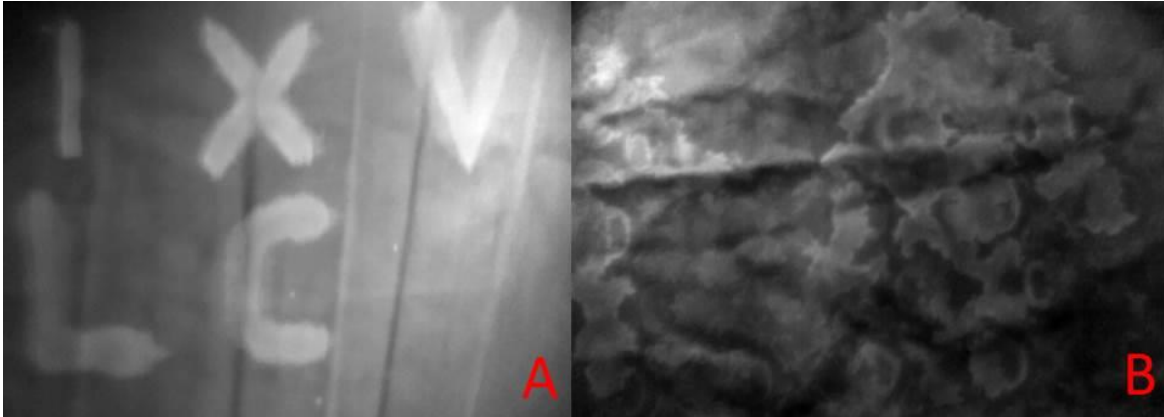
Figure 4.6 Here are range calculations for both measurements shown here. This can also be used to identify which area(s) was exposed to majority of the hot water vapor. Image A has a clear outline of each bloodstain that was deposited on the fabric. Image B shows the 1000x diluted bloodstain and the portion of the 100x stain that was within the camera's field of view.

4.4 CONCLUSION

In this process, we have identified a method to identify latent stains on fabrics without contaminating, manipulating, or damaging the sample. This process is simple in application yet complex because the number of different mechanisms controlling the response generated by water vapor exposure. While the latent heat thermography is not very selective, advances in IR camera technology make this technique very sensitive: small differences in temperature changes can be observed. Data processing techniques have been explored; however, most of these techniques have problems when applied to different samples. Further research should be done in this area to further understanding

38

and develop specific applications for this technique in industrial and forensic

applications.

BIBLIOGRAPHY

1. Brooke, H.; Baranowski, M.R.; McCutcheon, J.N.; Morgan, S.L.; Myrick, M.L. Multimode Imaging in the Thermal Infrared for Chemical Contrast Enhancement. Part 1: Methodology. *Analytical Chemistry*. **2010**, 82, 8412-8420.

2. Brooke, H.; Baranowski, M.R.; McCutcheon, J.N.; Morgan, S.L.; Myrick, M.L. Multimode Imaging in the Thermal Infrared for Chemical Contrast Enhancement. Part 2: Simulation Driven Design. *Analytical Chemistry*. **2010**, 82, 8421-8426.

3. Brooke, H.; Baranowski, M.R.; McCutcheon, J.N.; Morgan, S.L.; Myrick, M.L. Multimode Imaging in the Thermal Infrared for Chemical Contrast Enhancement. Part 3: Visualizing Blood on Fabrics. *Analytical Chemistry*. **2010**, 82, 8427-8431.

4. Fuzek, J.F. Absorption and Desorption of Water by some Common Fibers. *Industrial & Engineering Chemistry Product Research Development.* **1985**, 24, 140-144.

5. Gibson, P.; Rivin, D.; Kendrick, C.; Schreuder-Gibson, H. Humidity-Dependent Air Permeability of Textile Materials. *Textile Research Journal*. **1999**, 69, 311-317.

6. Hill, C.A.S.; Norton, A.; Newman, G. The Water Vapor Sorption Behavior of Natural Fibers. *Journal of Applied Polymer Science*. Sci. **2009**, 112, 1524-1537.

7. Fohr, J.P.; Couton, D.; Treguier, G. Dynamic Heat and Water Transfer Through Layered Fabrics. *Textile Research Journal*. **2002**, 72, 1-12.

8. Fan, J.; Cheng, X.Y. Heat and Moisture Transfer with Sorption and Phase Change through Clothing Assemblies: Part I: Experimental Investigations. *Textile Research Journal*. **2005**, 75, 99-105.

9. Fan, J.; Cheng, X.Y. Heat and Moisture Transfer with Sorption and Phase Change through Clothing Assemblies: Part II: Theoretical Modeling, Simulation, and Comparison with Experimental Results. *Textile Research Journal*. **2005**, 75, 187-196.

10. Indushekar, R.; Awasthi, P.; Gupta, R.K. Studies on Test methods used to measure Water Vapor Transmission of fabrics by DSC and Conventional Dish Techniques. *Journal of Industrial Textiles*. **2005**, 34, 223-242.

11. Le, C.V.; Ly, N.G. Multilayer Adsorption of Moisture in Wool and Its Application in Fabric Steaming. *Textile Research Journal*. **1992**, 62, 648-656.

12. Akiyama, G.; Matsuda, R.; Sato, H.; Hori, A.; Takata, A. Effect of functional groups in MIL-101 on water sorption behavior. *Microporous and Mesoporous Materials*. **2012**, 157, 89-93.

13. Vainer, B.G. Focal plane array based infrared thermography in fine physical experiment. *Journal of Physics D: Applied Physics.* **2008**, 41, 1-12.

14. Loskyll, J.; Stoewe, K.; Maier, W.F. Infrared thermography as a High-Throughput Tool in Catalysis Research. *ACS Combinatorial Science*. **2012**, 14, 295-303.

15. Campbell, N.; Reece, J.; Urry, L.; Cain, M.; Wasserman, S.; Minosky, P.; Jackson, R. *Biology*, 8th ed.; Pearson: San Francisco, CA, **2008**; pp. 911-915.

16. Donaldson, H.H. *The Rat: Reference Tables and Data*. Philadelphia, PA., 1915.

17. Bull, H.B. Adsorption of Water Vapor by proteins. *Journal of the American Chemical Society.* **1944**, 66 (9), 1499–1507.

APPENDIX A: MATLAB CODE

```matlab
function [oput1,oput2] = aom()
%This function calculates the amplitude of modulations. Must use Nick's LV
%program to acquire data. Acquire 10 cycles, off cycle first, using the
%solenoid for modulation. This programs calculates the average Ampltiude of
%modulation on the gold reflectance standard. The area choosen to average
%is an image of the gold standard. If you are to use this, change the
%'subx' area to enclose the gold standard; this will also change the last
%two for loops.
x=binarymovie;
subx=x(118:147,16:40,1:1200);
b=25;
t=90;
bref=zeros(1200,1);
tref=zeros(1200,1);
for i=1:9
    bref((b+1):(b+30),1)=1;
    b=b+120;
end

for i=1:9
    tref((t+1):(t+30),1)=1;
    t=t+120;
end

for i=1:30
    for j=1:25
        k=single_pixel(subx,i,j);
        bb=sum(k.*bref)/270;
        tt=sum(k.*tref)/270;
        oput2(i,j)=tt-bb;
    end
end
oput1=mean(mean(oput2));
end
```

```matlab
function [rawdata,roi]=read64bitimg
%Purpose: This function reads a binary file(that is 64bit floating point
precision)that is 614408 bytes. The first 8 bytes will be ignored. The next
part of the processing allocates the image to a 2D array. The next part
creates an image of the data

%By: O'Brien
%Updated: 11/28/2012

% Importing the bin file
[filename,pathname] = uigetfile('*.bin');
fullname = strcat(pathname,filename);
fid=fopen(fullname,'r','b');

fseek(fid,8,'bof'); %ignoring the 8bits of junk
```

41

```matlab
rawdata=zeros([240,320]);%preallocates a matrix for the image
rawdata=(fread(fid,[240,320],'float64'));
fclose('all');

roi=rawdata(1:240,120:200);%roi = region of interest
bkgrnd=mean([mean(roi(1:70,1:80)) mean(roi(170:240,1:80))])
signal=mean(mean(roi(71:155,1:80)))-bkgrnd
```

```matlab
function [data_final,introdat]=binarymovie
%This function reads binary data into matlab. This function is designed to
%be used when recording the steaming operation.
%Copied from HB's function / Updated by OBrien (1/20/13)
[filename,pathname] = uigetfile('*.bin');
fullname = strcat(pathname,filename);
fid=fopen(fullname,'r','b');

introdat=(fread(fid,[200,1],'uint16'));

fseek(fid,0,'eof');
n=(ftell(fid)-200)/(2*320*240);%n= the total number of frames.

% This code builds the 3D data array of images.
fseek(fid,200,'bof'); % There are 200 bits of "junk" data that we skip.
data=zeros(320, 240, n,'uint16'); % Preallocate for speed
for i=1:n
data(:,:,i)=(fread(fid,[240,320],'uint16'))';
end
fclose('all');
data_final = flipdim(double(data),2);%conversion to Double type of data
```

```matlab
function[]=framez(movie_data,speed)
%playmovie is used to play many frames that were acquired using the
%mothership labview program. In order to load the code into matlab, use the
%binarymovie.m file to load the frames into matlab. The playmovie.m
%function will find the size of the movie and allow a user to specify how
%fast the movie plays by inputting a 2nd integer that will tell the program
%how many frames to skip. If a 2nd number is not attached, the program will
%assume 1 is the speed.
[~,~,z]=size(movie_data);

for i=1:speed:z
    pcolor((movie_data(:,:,i))');
    colormap(gray);
    shading interp;
    title(num2str(i))
    pause
    drawnow
end
```

CUMULATIVE BIBLIOGRAPHY

1. Herschel, W. Experiments on the Refrangibility of the Invisible Rays of the Sun. *Royal Society of London*. **1800**, 90, 284-292.

2. Leslie, J. *An experimental Inquiry into the Nature and Propagation of Heat*; Bell and Bradfute: Edinburgh, 1804.

3. Olson, R.G. A note on Leslie's cube in the study of radiant heat. *Annals of Science*. **1969**, 25, 203-208.

4. Melloni, M. *Annal. Chim. Phys*.**1835,** 55, 337.

5. Bunsen, R.; Roscoe, H.E. Photochemische Untersuchungen. *Poggendorff's Ann. Chem. Phys*.**1957**, 100, 43-88.

6. Lockemann, G. The Centenary of the Bunsen Burner. *Journal of Chemical Education*. **1956,** 33, 20-22.

7. Kirchhoff, G.; Bunsen, R. *Poggendorff's Ann. Phys. Chem*. **1860**, 110, 161.

8. Wolfe, W.L. *Handbook of Military Infrared Technology*; Government Printing Office: Washington, DC, 1965; pp 31-56.

9. Pfund, A.H. The Electric Welsbach Lamp. *Journal of Optical Spectroscopy of America*. 1936, 26, 439-442.

10. Barnes, R.B.; Bonner, L.G.A Survey of Infra-Red Spectroscopy. *Journal of Chemical Education*. **1937,** 14, 564-571.

11. Nernst, W.; Bose, B. The theory of Auer Light. *Physics Zeits*, **1900**, 1, 289-291.

12. Coblentz, W.W. *Investigations into Infrared Spectra Part VII*. Carnegie Institution of Washington: Washington, DC, 1905.

13. Registration number 0200201 to the Wireless Resistor Company of America, now registered to Sandvik Wire and Heating Technology Corporation.

14. Strong, J Procedures in Experimental Physics (Prentice Hall Inc. New York 1938), pp 348.

15. Cann, M.W.P. Light Sources in the 0.15-20-µ Spectral Range. *Applied Optics*. **1969,** 1645-1661.

16. McCluney, R. *Introduction to Radiometry and Photometry*; Artech House: Boston, MA; 1994; pp. 79.

17. Brooke, H.; Baranowski, M.R.; McCutcheon, J.N.; Morgan, S.L.; Myrick, M.L. Multimode Imaging in the Thermal Infrared for Chemical Contrast Enhancement. Part 1: Methodology. *Anal Chem.* **2010**, 82, 8412-8420.

18. Brooke, H.; Baranowski, M.R.; McCutcheon, J.N.; Morgan, S.L.; Myrick, M.L. Multimode Imaging in the Thermal Infrared for Chemical Contrast Enhancement. Part 2: Simulation Driven Design. *Anal. Chem.* **2010**, 82, 8421-8426.

19. Brooke, H.; Baranowski, M.R.; McCutcheon, J.N.; Morgan, S.L.; Myrick, M.L. Multimode Imaging in the Thermal Infrared for Chemical Contrast Enhancement. Part 3: Visualizing Blood on Fabrics. *Anal. Chem.* **2010**, 82, 8427-8431.

20. Koerperick, E.J.; Norton, D.T.; Olesberg, J.T.; Olson, B.V.; Prineas, J.P.; Boggess. T.F. Cascaded Superlattice InAs/GaSb Light-Emitting Diodes for Operation in the Long-Wave Infrared. *IEEE Journal of Quantum Electronics*. **2011,** 47, 50-54.

21. Das, N.C. Performance Comparison of Top- and Bottom-emitting Long Wave Infrared Light Emitting Diode Devices. *Journal of Electronic Materials*. **2009,** 38, 2329-2334.

22. Das, N.C.; Bradshaw, J.; Towner, F.; Leavitt, R. Long-wave (10 µm) infrared light emitting diode device performance. *Solid-State Electronics*. **2008,** 52, 1821-1824.

23. Giraud, S.O.C.; Hasko, D.G. Mesoscale thermal infrared sources. Microelectronic Engineering. **1998,** 41-42, 579-582.

24. Bauer, D.; Heeger, M.; Gebhard, M.; Benecke, W. Design and fabrication of a thermal infrared emitter. *Sensors and Actuators A*. **1996**, 55, 57-63.

25. Laine, D.C.; Al-Jourani, M.M.; Carpenter, S.; Sedgbeer, M. Pulsed wideband IR thermal source. *IEE Proceedings-Optoelectronics*. **1997**, 144, 315-322.

26. Kwon, B.; Schulmerich, M.V.; Bhargava, R.; King, W.P. Infrared Emission from Heated Microcantilevers. *Nanoscale and Microscale Thermophysical Engineering*. **2013,** 17, 141-153.

27. Yue, F.; Tomm, J.W.; Kruschke, D.; Glas, P.; Bzheumikhov, K.A.; Margushev, Z.C. PbS:Glass as broad-bandwith near-infrared light source. *Optics Express*. **2013,** 21, 2287-2295.

28. Tu, J.; Howard, D.; Collins, S.D.; Smith, R.L. Micromachined, silicon filament light source for spectrometric microsystems. *Applied Optics*. **2003,** 42, 2388-2397..

29. Inoue, T.; Asano, T.; Zoysa, M.D.; Oskooi, A.; Noda, S. Design of single-mode narrow-bandwidth thermal emitters for enhanced infrared light sources. *Applied Physics Letters*. **2013,** 30, 165-172.

30. Tsai, M.W.; Chuang, T.H.; Meng, C.Y.; Chang, Y.T.; Lee, S.C. High Performance Midinfrared narrow-band plasmonic thermal emitter. *Applied Physics Letters*. **2006,** 89, 1731161-1731163.

31. Capasso, F. High-performance midinfrared quantum cascade lasers. *Optical Engineering*. **2010,** 49, 111102-1111029.

32. Troccoli, M.; Wang, X.; Fan, J. Quantum cascade lasers: high-power emission and single-mode operation in the long-wave infrared (λ>6 µm). *Optical Engineering*. **2010,** 49, 1111061-1111069.

33. Rogalski, A. History of infrared detectors. *Opto-Electronics Review*. **2012**, 20(3), 279-308.

34. Kateb, B.; Yamamoto, V.; Yu, C; Grundfest, W.; Gruen, J.P. Infrared Thermal Imaging: a review of the literature and case report. *NeuroImage*. **2009**, 47, T154-T162.

35. Bagavathiappan, S.; Lahiri, B.B.; Saravanan, T.; Philip, J.; Jayakumar, T. Infrared Thermography for condition monitoring – A review. *Infrared Physics & Technology*. **2013**, 60, 35-55.

36. Verhoeven, G. Imaging the invisible using modified digital cameras for straightforward and low-cost archaeological near-infrared photography. *Journal of Archaeological Science.* **2008**, 35, 3087-3100.

37. Peng, D.; Jones, R. Lock-in thermographic inspection of squats on rail steel head. *Infrared Physics & Technology*. **2013**, 57, 89-95.

38. Lahiri, B.B.; Bagavathiappan, S.; Jayakumar, T.; Philip, J. Medical Applications of infrared thermography: A review. *Infrared Physics & Technology*. **2013**, 55, 221-235.

39. Deans, J.; Gerhard, J.; Carter, L.J. Analysis of a thermal imaging method for landmine detection, using infrared heating of the sand surface. *Infrared Physics & Technology*. **2006**, 48, 202-216.

40. Safitri, A.; Mannan, M.S. Methane Gas visualization Using Infrared Imaging System and Evaluation of Temperature Dependence of Methane Gas Emissivity. *Industrial & Engineering Chemistry Research*. **2010**, 49(8), 3926-3935.

41. Horny, N. FPA camera standardization. *Infrared Physics & Technology*. **2003**, 44, 109-119.

42. Bower, S.M.; Kou, J.; Saylor, J.R. A method for the temperature calibration of an infrared camera using water as a radiative source. *Review of Scientific Instruments*. **2009**, 80(9), 1-7.

43. Gauthier Jr., L.R.; Howser, L.M.; Prendergast, D.T.; Mattix, M.P. Radiometric dynamic scene processing for uncooled IRFPAs. In *SPIE Proceedings 1996*, Proceedings of the Infrared Imaging Systems: Design, Analysis, Modeling, and Testing XVII, Orlando, FL, April 17, 2006.

44. Mermelstein, M.D.; Snail, K.A.; Priest, R.G. Spectral and radiometric calibration of midwave and longwave infrared cameras. *Optical Engineering*. **2000**, 39, 347-352.

45. Rice, J.P.; Lykke, K.R.; Yoon, H.W. A method for testing the spectral responsivity of infrared cameras using tunable lasers. Proc. SPIE 5076, Infrared Imaging Systems: Design, Analysis, Modeling, and Testing XIV, 112 (August 25, 2003); doi:10.1117/12.487113.

46. FLIR A315 / A615 Thermal Camera Technical Specifications – FLIR. http://www.flir.com/cs/emea/en/view/?id=41955 (accessed June 27, 2013).

47. Fuzek, J.F. Absorption and Desorption of Water by some Common Fibers. *Industrial & Engineering Chemistry Product Research Development.* **1985**, 24, 140-144.

48. Gibson, P.; Rivin, D.; Kendrick, C.; Schreuder-Gibson, H. Humidity-Dependent Air Permeability of Textile Materials. *Textile Research Journal*. **1999**, 69, 311-317.

49. Hill, C.A.S.; Norton, A.; Newman, G. The Water Vapor Sorption Behavior of Natural Fibers. *Journal of Applied Polymer Science*. Sci. **2009**, 112, 1524-1537.

50. Fohr, J.P.; Couton, D.; Treguier, G. Dynamic Heat and Water Transfer Through Layered Fabrics. *Textile Research Journal*. **2002**, 72, 1-12.

51. Fan, J.; Cheng, X.Y. Heat and Moisture Transfer with Sorption and Phase Change through Clothing Assemblies: Part I: Experimental Investigations. *Textile Research Journal*. **2005**, 75, 99-105.

52. Fan, J.; Cheng, X.Y. Heat and Moisture Transfer with Sorption and Phase Change through Clothing Assemblies: Part II: Theoretical Modeling, Simulation, and Comparison with Experimental Results. *Textile Research Journal*. **2005**, 75, 187-196.

53. Indushekar, R.; Awasthi, P.; Gupta, R.K. Studies on Test methods used to measure Water Vapor Transmission of fabrics by DSC and Conventional Dish Techniques. *Journal of Industrial Textiles*. **2005**, 34, 223-242.

54. Le, C.V.; Ly, N.G. Multilayer Adsorption of Moisture in Wool and Its Application in Fabric Steaming. *Textile Research Journal*. **1992**, 62, 648-656.

55. Akiyama, G.; Matsuda, R.; Sato, H.; Hori, A.; Takata, A. Effect of functional groups in MIL-101 on water sorption behavior. *Microporous and Mesoporous Materials*. **2012**, 157, 89-93.

56. Vainer, B.G. Focal plane array based infrared thermography in fine physical experiment. *Journal of Physics D: Applied Physics.* **2008**, 41, 1-12.

57. Loskyll, J.; Stoewe, K.; Maier, W.F. Infrared thermography as a High-Throughput Tool in Catalysis Research. *ACS Combinatorial Science*. **2012**, 14, 295-303.

58. Campbell, N.; Reece, J.; Urry, L.; Cain, M.; Wasserman, S.; Minosky, P.; Jackson, R. *Biology*, 8th ed.; Pearson: San Francisco, CA, **2008**; pp. 911-915.

59. Donaldson, H.H. *The Rat: Reference Tables and Data*. Philadelphia, PA., 1915.

60. Bull, H.B. Adsorption of Water Vapor by proteins. *Journal of the American Chemical Society.* **1944**, 66 (9), 1499–1507.